Laser heat treatments driven by integrated beams: role of irradiation nonuniformities

José-Luis Ocaña, Angel García-Beltrán, Ferran Laguarta, Jesús Armengol, Núria Lupón, and Fidel Vega

An analysis is given of how nonuniformities in the laser beam intensity translate into variations on the induced temperature distribution on an irradiated sample. The study involves materials with different thermal conductivities. By use of a reshaped irradiating beam obtained with a multifaceted integrating mirror, a three-dimensional numerical calculation allows us to establish both surface and in-depth temperature distributions. The results show that in the case of materials such as glass (i.e., with low thermal conductivity) large thermal gradients occur both on the surface and in depth during irradiation. However, the lateral heat flow is high enough to strongly reduce the surface gradients as soon as the laser irradiation ends. Conversely, in good thermal conductors such as nickel, the laser intensity nonuniformities induce a thermal peaking of the surface with lateral thermal gradients that are by no means negligible. Experimental evidence during laser glass polishing that confirms the numerical assessments are also provided.

OCIS codes: 140.3390, 140.6810, 160.2750, 140.3300, 220.5450, 120.6660.

1. Introduction

Many applications involving laser beam irradiation of a sample require uniform irradiance patterns at the surface plane. Such applications include both laser materials processing and laser–material interaction studies. Thus successful surface modification processes such as transformation hardening, bulk surface alloying, cladding, and laser glazing require that the surface be brought to a narrow temperature gap. Even small deviations in laser intensity will result in inadequate final properties of the irradiated surface. The effects of lack of uniformity in the laser beam are even worse in laser applications that involve materials with a low thermal conductivity, for example, ceramics, crystals, or glasses.

Monomode and multimode laser beams have nonuniform transverse intensity distributions, and it is necessary to reshape them to achieve smooth intensity patterns. Different methods of obtaining flat-topped intensity distributions from nonuniform (mainly Gaussian) low-power laser beams have been proposed in recent years: aspherical lenses,[1] diffractive systems,[2–4] and absorbing filters.[5,6] With high-power Nd:YAG or CO_2 laser applications beam shaping was carried out recently with so-called active devices[7,8] or more recently by means of commercial multifaceted mirrors[9,10] and pipe light guides or kaleidoscopes.[11,12] Multifaceted mirrors use a single reflection of a laser beam from a segmented aperture that provides a high reflection efficiency, but they are difficult to manufacture, and their cost is high. Pipe light guides reshape the incoming diverging beam by means of multiple reflections from the inside walls of the pipe. They exhibit a lower reflection efficiency, and the actual number of reflections involves a compromise between beam uniformity and beam energy losses. Nevertheless, pipe light guides are easier to fabricate and have a lower cost than multifaceted mirrors.

These two kinds of reflective integrating device provide at their best integration plane theoretic flat-topped intensity distributions produced by the superposition of the different portions of the segmented laser wave fronts. However, today most laser material processing applications are driven by unstable cavity laser sources that provide nearly pure transverse monomode beams with a large spatial coher-

J.-L. Ocaña and A. García-Beltrán are with the Escuela Técnica Superior de Ingenieros Industriales, Universidad Politécnica (Madrid), c/José Gutiérrez Abascal 2, 28006 Madrid, Spain. F. Laguarta, J. Armengol, N. Lupón, and F. Vega are with the Departament d'Òptica i Optometria, Universitat Politècnica de Catalunya, c/Violinista Vellsolà 37, 08222 Terrassa, Spain. The e-mail address for F. Vega is fvega@oo.upc.es.

Received 7 December 1998; revised manuscript received 26 April 1999.

0003-6935/99/214570-07$15.00/0

ence. The application of multifaceted mirrors or pipe light guides to highly coherent laser beams results in real nonuniform intensity distributions that show sharp contrast interferential effects.

In this paper we study the laser surface heat treatment process driven by coherent laser beams with nonuniform intensity distributions obtained with multifaceted integrating mirrors. Special attention is paid to the effects of laser beam inhomogeneities that may translate, depending on the irradiation parameters (namely, intensity distribution and irradiation time) and the material properties (mostly thermal conductivity), into a nonuniform temperature distribution on the sample. A three-dimensional finite-element numerical model is used to calculate the spatial and the temporal temperature distributions induced on the treated samples. The results show that the induced surface thermal gradients are of major importance in the case of materials with relatively low thermal conductivity, such as glass, and are also significant in the case of materials that are regarded as good thermal conductors, such as nickel. These results are compared with the experimental ones obtained in optical glass samples irradiated with a CO_2 coherent laser beam reshaped by means of a 6×6 faceted mirror. Evidence of the effects of laser-induced thermal nonuniformities during laser polishing of optical glass samples are given.

2. Multifaceted Integrating Mirrors

A conventional faceted mirror is composed of an array of reflecting flat facets whose centers lie on a conic surface. Each facet reflects a part of a collimated incoming laser beam, the different portions of this segmented beam (referred to hereafter as beamlets) overlapping at the focal plane where the sample is usually located. In this way a beam average occurs at the focal plane, each facet contributes with a beamlet, and their combined sum (without including the interferential effects) leads to a more uniform intensity distribution.[9,10] Among other parameters the beam uniformity achieved depends on the number of facets that participate in the integration; the higher the latter, the higher the uniformization obtained. Therefore a beam expander is usually used to illuminate the faceted mirror. Moreover, long-duration high-power laser treatments can require a cooling system for avoiding undesired heating of the mirror. Another intrinsic limitation of these integrators is that the beam size at the focal plane is reduced to the size of a facet. As a result, in applications in which a higher or a lower magnification is required and/or the sample is not located at the focal plane of the mirror, an imaging system must be used.

The experimental setup used for irradiation was previously described in Ref. 13. It consists of a spherical molybdenum-coated 6×6 faceted mirror (focal length, 500 mm). The facets are flat squares of 8×8 mm^2. The coherent CO_2 laser beam ($\lambda = 10.6$ μm) has a transverse intensity distribution corresponding approximately to a TEM_{00} mode. A beam expander ($5\times$ magnification) is used to illuminated

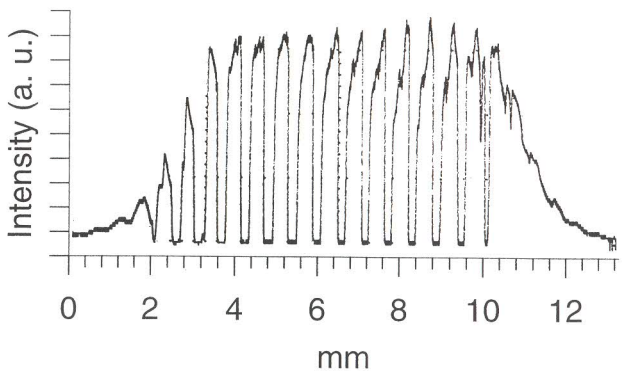

Fig. 1. Experimental laser intensity profile obtained at the sample plane with a 6×6 multifaceted integrating mirror. To have a good spatial resolution, we recorded the profile by scanning the laser intensity distribution along a line with a pinhole positioned in front of a pyroelectric detector.

the whole faceted mirror, and the irradiated sample is located at the focal plane of the mirror. Figure 1 shows a measured laser intensity profile obtained at the sample plane, and, as mentioned above, it corresponds to a sharp interferential pattern, because of the overlapping of the beamlets at the sample plane.

To calculate the laser integrated intensity distribution that corresponds to the experimental conditions described above, one must add coherently the contribution of each facet of the multifaceted mirror in the form

$$I(x, y) = \left| \sum_{n=1}^{36} A_n(x, y) \exp\{ik[\pm x \sin(\alpha_n) \pm y \sin(\beta_n)]\} \right|^2, \quad (1)$$

where $A_n(x, y)$ is the amplitude of any of the beamlets at the sample plane and α_n and β_n are the angles formed by the wave front of the beamlet and the sample plane in the x and the y directions, respectively.

Figure 2 shows the calculated regularly peaked interference pattern. The resulting interfringe is $d = 0.66$ mm, whereas the visibility of the pattern is nearly 100%. These features (namely, interfringe and visibility) depend on the laser wavelength, the focal length of the faceted mirror, the number of facets that participate in the beam integration, and the laser beam mode. Thus the interfringe is determined with the formula $\lambda/2\phi$ (ϕ being the angle between the facets), whereas the number of facets governs the finesse of the interference pattern: The higher the number of facets, the higher the finesse. Therefore, contrary to what happens when noncoherent laser beams are used, a greater number of facets do not increase the beam uniformity.

The comparison between experimental (Fig. 1) and simulated results [Fig. 2(b)] reveals good qualitative agreement at the center of the profile (experimental interfringe of 0.6 mm and nearly 100% of fringe visibility). However, at the queues the experimental profile shows a clear decrease in the intensity that is not present in the simulations. This difference can

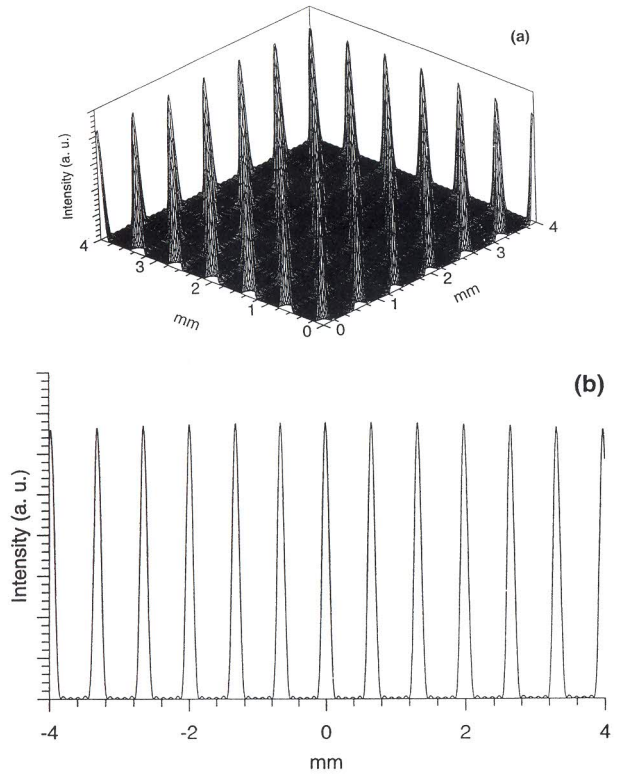

Fig. 2. (a) Calculated laser intensity distribution and (b) intensity profile along a line passing through the intensity maxima at the sample plane. Results are obtained with application of Eq. (1) and correspond to a 6 × 6 multifaceted integrating mirror. For the sake of clarity only half of the intensity distribution is shown.

be explained by the fact that the calculations were performed without inclusion of several tolerances that are inherent to the design of a multifaceted mirror. Thus the tilt angle required for separation of the incoming beam from the reflected beamlets and/or any misalignment of the facets with respect to the conic surface of the mirror alter the overlapping of the beamlets at the sample plane, which induces both an edge roll-off and a distortion of the integrated intensity distribution. Moreover, the misalignment of the facets also induces a small phase change among the beamlets that generates a low-frequency moiré pattern. Another related effect is caused by errors in the location of the facets (piston) that induce random path phase differences among the beamlets, and as a consequence the interferential pattern becomes more complex. Finally, diffraction effects at the edge of the facets can contribute to notorious intensity modulations in the sample plane. Since there are several edges, the diffraction contributions add coherently and affect preferentially the queues of the intensity distribution (see Fig. 1).

3. Numerical Temperature Calculations

Much work has been done toward understanding the heat-conduction process during laser heating carried out with both stationary and scanning beams.[14] When a stationary beam is used, the laser-induced heating process can be well described within a thermal model that is based on the three-dimensional heat-flow equation given by

$$\rho c_p \frac{\partial T}{\partial t} = \frac{\partial}{\partial x}\left(\kappa \frac{\partial T}{\partial x}\right) + \frac{\partial}{\partial y}\left(\kappa \frac{\partial T}{\partial y}\right) + \frac{\partial}{\partial z}\left(\kappa \frac{\partial T}{\partial z}\right) + P(x, y, z, t), \quad (2)$$

where x and y are the spatial coordinates at the sample surface, z is the distance to the surface along the surface normal, t is the time, c_p is the specific heat, ρ is the density, and κ is the thermal conductivity. The source term $P(x, y, z, t)$ is the part of the laser power/unit volume that is absorbed by the irradiated material (either glass or nickel). Under the assumption of a perpendicularly incident laser beam of irradiance $I_{\text{laser}}(x, y, t)$ at the sample plane, the power density is[15]

$$P(x, y, z, t) = (1 - R)I_{\text{laser}}(x, y, t)\alpha \exp(-\alpha z), \quad (3)$$

where R is the reflectivity and α is the absorption coefficient (both at the irradiation wavelength). It must be noted that both glass and nickel present a high absorption coefficient at the 10.6-μm laser wavelength. When we deal with materials with low values of the absorption coefficient, it could be necessary to modify Eq. (3) to include self-focusing effects that would cause high subsurface irradiance.[16]

To obtain the sample temperature distribution $T(x, y, z, t)$ from Eq. (2), a numerical code based on the finite-element method was developed. The material is considered homogeneous in the form of a slab between the planes $z = 0$ and $z = L$, L being the sample thickness. The sample is divided into $i \times j \times l$ elements of volume $\Delta x \times \Delta y \times \Delta z$ and is taken to be at a uniform initial temperature T_o which is added to the calculated temperature. The boundary conditions are those corresponding to a thermally insulated solid; i.e., no heat flow across the boundaries is allowed. This means that the temperature distribution $T(x, y, z, t)$ must satisfy the condition

$$\left(\frac{\partial T}{\partial z}\right) = 0 \text{ for } z = 0, \qquad z = L \text{ at all times.} \quad (4)$$

Further details on the numerical code can be found elsewhere.[17]

Heat-flow simulation was first used to calculate the temperature distribution induced in materials of low thermal conductivity, such as optical glass, where laser polishing was previously reported.[13,18,19] To emphasize the effect that the local inhomogeneities in the laser beam induces on the thermal dynamics of the sample, a comparative analysis was carried out between a uniform intensity distribution and a regularly peaked one (the latter reproducing the interferential intensity pattern experimentally obtained with the multifaceted mirror).

The thermal and the optical parameters used were taken from Refs. 20–23 and are summarized in Table 1. The laser intensity distributions are included in Table 2.

Figure 3 shows the resulting temperature distribu-

Table 1. Thermal and Optical Parameters of B-270 Optical Glass and Nickel[a]

Parameter	Material	
	B-270 Optical Glass	Nickel
ρ (kg m^{-3})	2.5×10^3	8.89×10^3
c_p (J Kg^{-1} K^{-1})	10^3	437.5
κ (W m^{-1} K^{-1})	$1.047 + 0.001489 \times T^b$ ($T < 900$ °C)	
	2.387 ($T > 900$ °C)	91.5
α (m^{-1})	7.1×10^{-4}	$\sim\infty$
R	0.2	0.98

[a]Parameters listed are density (ρ), specific heat (c_p), thermal conductivity (κ), absorption coefficient (α), and reflectivity R. Both α and R are determined at the irradiation wavelength λ = 10.6 μm.
[b]T is in degrees Celsius.

tion on the glass surface irradiated with the uniform laser beam. As expected, at the end of the irradiation a uniform temperature is reached all over the laser spot, although the presence of lateral surface heat flow during the irradiation time is also evident. This accounts for the smooth temperature decreases obtained immediately outside the irradiated area.

Table 2. Laser Intensity Distributions Used in Thermal Calculations[a]

	Calculation	Absolute Value of x	Absolute Value of y
Uniform	P_o/xy	$\leq l/2$	$\leq l/2$
	0	$\geq l/2$	$\geq l/2$
Peak patterned	$I_o \sin^8[(\pi/d)x] \times \sin^8[(\pi/d)y]$	$\leq l/2$	$\leq l/2$
	0	$\geq l/2$	$\geq l/2$

[a]P_o (W) is the absorbed laser power, l (mm) is the square spot size, d is the interfringe (mm), and I_o (W/cm^2) is the maximum intensity. To obtain an average power of P_o when we integrate the peak patterned distribution over the spot area (l^2), I_o is obtained as $P_o/(35/128)^2 l^2$.

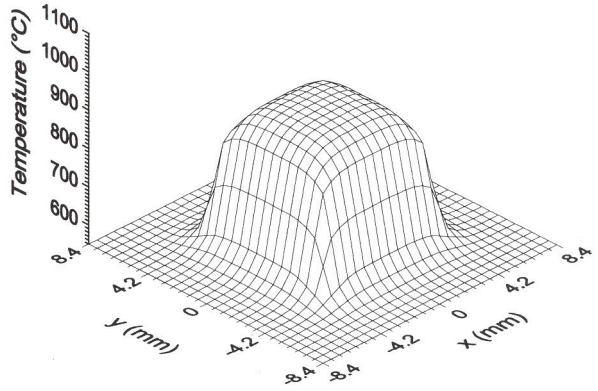

Fig. 3. Simulated surface temperature distribution on a 5-mm-thick, surface-infinite slab of B-270 optical glass preheated to T_o = 550 °C. Calculations are performed with the uniform intensity distribution. Results are obtained with P_o = 72.5 W and l = 8.4 mm. The irradiation time was 1.5 s.

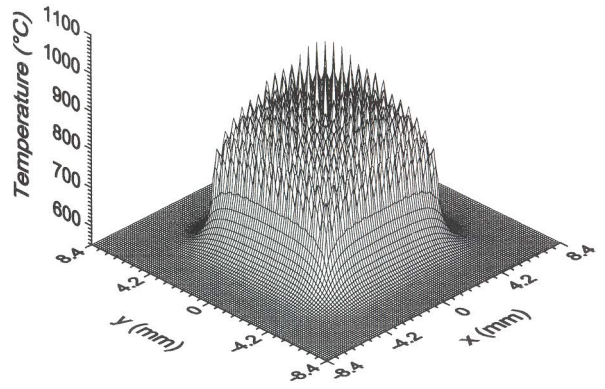

Fig. 4. Simulated surface temperature distribution on a 5-mm-thick, surface-infinite slab of B-270 optical glass preheated to T_o = 550 °C. Calculations are performed with the peak patterned intensity distribution. Results are obtained with P_o = 72.5 W and l = 8.4 mm. The irradiation time was 1.5 s.

Figure 4 gives the surface temperature calculated when the peak patterned intensity is used. The results show that thermal spikes are induced at the surface locations where the maxima of the intensity distribution are applied. This indicates that, unlike in the former case, steeper thermal gradients both laterally and in depth should be induced under these conditions.

To check this statement, the thermal cycles (heating plus cooling) were calculated throughout the depth of the glass. Figure 5 shows the in-depth temperature curves for the uniform irradiation condition, whereas Fig. 6 corresponds to the temperatures calculated under a surface point that receives a maximum of the peak patterned distribution.

Inspection of both sets of results allows us to establish significant differences between the thermal conditions reached in either case. First, the maxi-

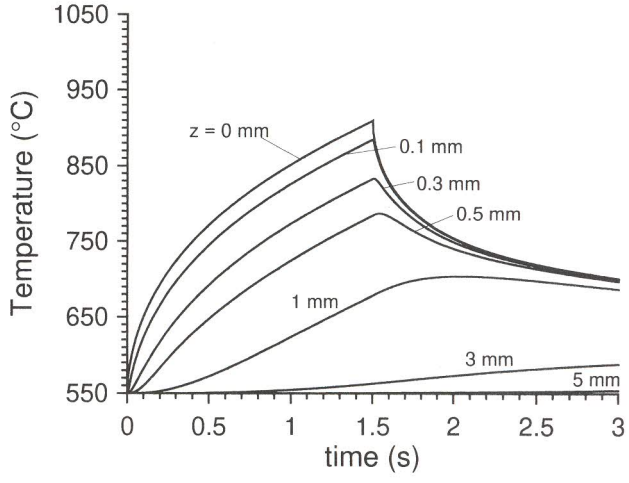

Fig. 5. Calculated in-depth temperatures as a function of time obtained on a 5-mm-thick, surface-infinite slab of B-270 optical glass preheated to T_o = 550 °C. Results correspond to the uniform laser intensity distribution with P_o = 72.5 W, spot size l = 8.4 mm, and irradiation time t = 1.5 s.

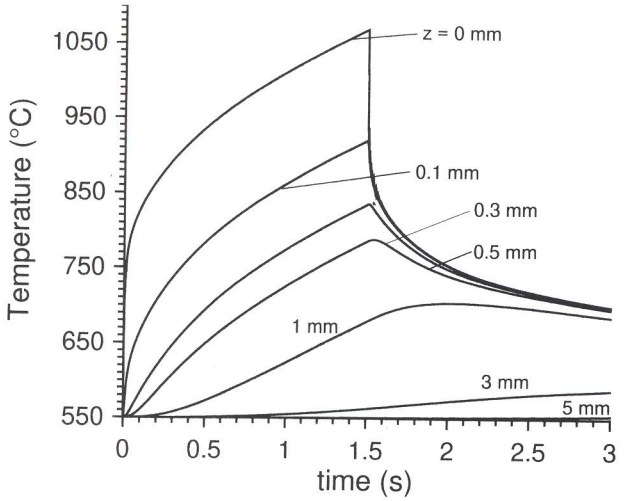

Fig. 6. Calculated in-depth temperatures as a function of time obtained on a 5-mm-thick, surface-infinite slab of B-270 optical glass preheated to T_o = 550 °C. Results correspond to the peak patterned laser intensity distribution with P_o = 72.5 W, spot size l = 8.4 mm, and irradiation time t = 1.5 s. Calculations are carried out under a surface point that receives a maximum of intensity.

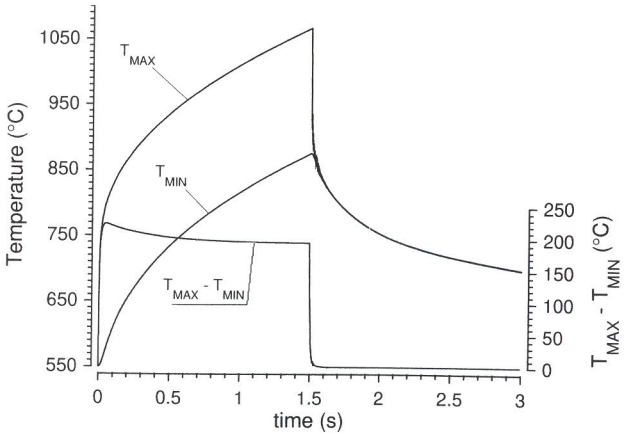

Fig. 7. Calculated surface temperature curves (scale on left-hand side) as a function of time in a 5-mm-thick, surface-infinite slab of B-270 optical glass preheated to T_o = 550 °C and irradiated with the peak patterned laser intensity distribution. Temperature curves labeled T_{MAX} and T_{MIN} correspond to adjacent surface points that receive either a maximum or a minimum of intensity. The temperature difference between these points as a function of time (curve labeled $T_{MAX} - T_{MIN}$, right-hand axis) is also included. The irradiation parameters were P_o = 72.5 W, spot size l = 8.4 mm, and irradiation time t = 1.5 s.

mum temperature values obtained on the sample surface (temperature curve with z = 0) are clearly higher in the case of the peak patterned intensity distribution (for the particular conditions shown, 900 °C in the uniform irradiation case versus 1060 °C in the peak patterned irradiation). Second, much stronger in-depth thermal gradients are developed in the latter case. Thus steep thermal gradients of ~1500 °C mm^{-1} are calculated from Fig. 6, versus 150 °C mm^{-1} obtained in the case of the uniform irradiation distribution (Fig. 5). In connection with this, extreme differences can be noted between the cooling rates of points at the glass surface in the two situations considered: Whereas in the case of the uniform beam a cooling rate of 1584 °C s^{-1} is obtained for all the points on the surface, in the case of the peak patterned intensity distribution, cooling rates ranging from 7600 to 324 °C s^{-1} are found, depending on whether the surface point receives a maximum or a minimum, respectively, of intensity.

Concerning lateral surface thermal gradients developed when the peak patterned intensity distribution is applied, Fig. 7 shows the calculated thermal cycles of two neighboring surface points that receive either a maximum or a minimum of intensity (i.e., two points on the surface that are separated by one half of the interfringe). It is clear from this figure that the temperature differences between surface points are established as soon as the irradiation starts. In the calculated conditions the maximum temperature difference obtained is higher than 200 °C, which leads to a very steep lateral surface gradient (greater than 650 °C mm^{-1}). However, it should be noted that, although glass is a material with a low thermal conductivity, the lateral heat flow is high enough to average out the surface temperature differences immediately after the laser irradiation ends. In others words, both temporal and spatial thermal gradients on the glass surface will persist only during the irradiation time. This is a striking result, since it shows that, despite the inherent difficulty of the glass to redistribute the absorbed energy, its thermal conductivity is high enough to allow for a fast reduction time (compared with the irradiation time) of the thermal gradients induced by local nonuniformities in the irradiation intensity distribution.

In the same way it could be asked whether materials that typically exhibit a high thermal conductivity, such as metals, are truly able to minimize the occurrence of significant thermal gradients on irradiation with a nonuniform laser intensity distribution.

Figure 8 shows the calculated surface temperature distribution obtained in a sample of nickel irradiated with the peak patterned laser intensity distribution. The laser power was adjusted to obtain an identical maximum surface temperature to that of glass with the same irradiation time. Comparing this with the results obtained for glass (Fig. 4), we see that the temperature distribution for nickel registers greater differences between the average temperature at the center and at the periphery of the irradiated area. This accounts for the greater ability of the nickel for lateral heat transfer during the irradiation time, the surroundings of the irradiated area acting as an efficient thermal sink. However, Fig. 8 also shows that, as with glass, a thermal peaking of the surface is obtained despite the much higher thermal conductivity of this metal.

This is more clearly seen in Fig. 9, where the thermal cycles of two neighboring surface points that receive either a maximum or a minimum of the laser intensity are shown. Although the maximum sur-

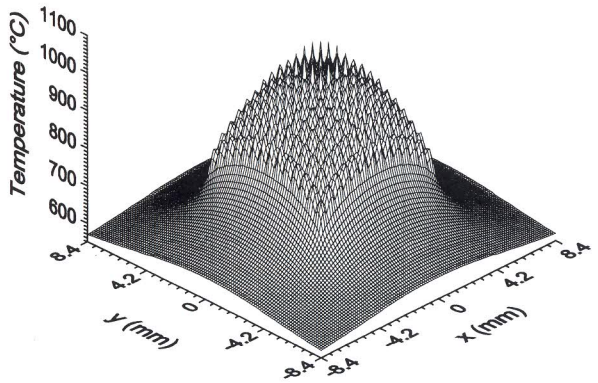

Fig. 8. Simulated surface temperature distribution on a 5-mm-thick, surface-infinite slab of nickel preheated to T_o = 550 °C. Calculations are performed with the peak patterned intensity distribution. Results are obtained with P_o = 800 W and spot size l = 8.4 mm. The irradiation time was t = 1.5 s.

face temperature differences, and thus the resulting surface thermal gradients, are obviously lower than in the case of glass (see Fig. 7), they are by no means negligible (250 °C mm^{-1} in the reported conditions).

4. Experimental Results

Laser polishing of glass occurs, since the laser-surface heat treatment promotes the softening of a thin layer of the glass surface that flows under the action of the surface tension.[13,19] The ability of the glass surface to flow depends on the reduction of the coefficient of viscosity, which becomes temperature dependent. Our calculations show that significant temperature differences that persist during the irradiation time can be expected between points on the surface of the glass on irradiation with a peak patterned laser intensity distribution. In particular, by use of a relatively short irradiation time (see Fig. 7), only the surface points that receive a maximum of the laser intensity achieve a temperature that exceeds the one for glass flow (≳1000 °C). As a consequence, only at these surface points should noticeable surface-tension-driven flow occur. Experimental confirmation of this assessment is provided in Fig. 10, which shows the appearance of an irradiated glass surface. There is an array of surface points where a mass flow has taken place. Since these points are separated by ≈0.67 mm (i.e., a distance very close to the experimentally determined peak patterned interfringe), they undoubtedly correspond to the maxima of intensity of the integrated laser distribution. The rest of the surface was not heated sufficiently to allow for a significant surface flow and thus remains almost unaffected.

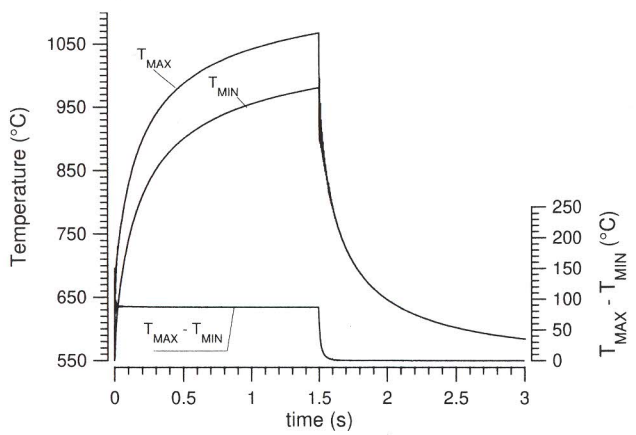

Fig. 9. Calculated surface temperature curves (scale on left-hand side) as a function of time in nickel preheated to 550 °C and irradiated with the peak patterned laser intensity distribution. Temperature curves labeled T_{MAX} and T_{MIN} correspond to adjacent surface points that receive either a maximum or a minimum of intensity. The temperature difference between these points as a function of time (curve labeled $T_{MAX} - T_{MIN}$, right-hand axis) is also included. The irradiation parameters were P_o = 800 W, spot size l = 8.4 mm, and irradiation time t = 1.5 s.

Fig. 10. Optical image of the surface of the B-270 optical glass after irradiation with a laser intensity distribution obtained by means of a 6 × 6 faceted integrating mirror. To avoid thermal cracking, the sample was preheated prior to the laser treatment to T_o = 550 °C. The irradiation was carried out with P_o = 72.5 W, spot size l = 8.4 mm, and irradiation time t = 1.5 s.

When the total energy deposited at the glass sample is increased, the coefficient of viscosity is reduced over the whole of the irradiated area, thus allowing for a global flow process with a dramatic lowering of the surface roughness.[13,19] Interferometric inspection of the samples irradiated in these conditions shows that in addition to the polishing of the surface there is an associated hill-shaped plastic deformation (Fig. 11), an effect that has been exploited recently to fabricate micro-optical components.[24,25] This surface deformation occurs preferentially at those points that receive a maximum of the laser intensity. Since these points become hotter, they undergo a higher thermal expansion. Moreover, because of the lowering of the density of the viscous glass with temperature, the hotter surface points tend to achieve a greater volume, which enhances the surface deformation process as previously reported during irradiation of viscous liquids with Gaussian laser beams.[26,27] In the case of glass our calculations demonstrate that the irradiation process induces steep depth temperature gradients with

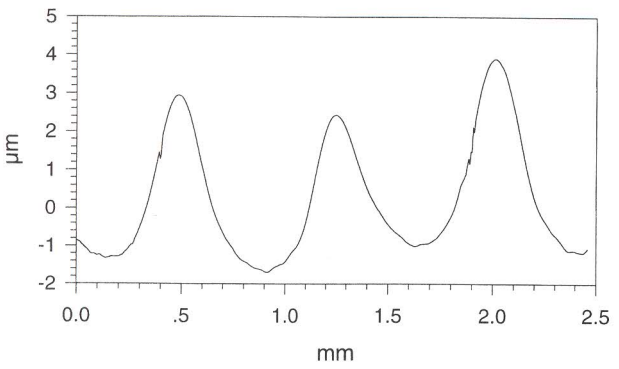

Fig. 11. Glass surface profile after irradiation with a laser intensity distribution obtained by means of a 6 × 6 faceted integrating mirror. To avoid thermal cracking, the sample was preheated prior to the laser treatment to T_o = 550 °C. The irradiation was carried out with P_o = 50 W, spot size l = 8.4 mm, and irradiation time t = 3 s. The surface profile was obtained with a commercial phase-shifting optical profiler with a 2.5× objective featuring a Michelson interferometer.

fast cooling rates. As a consequence, the viscoelastic expansion of the hotter surface points can freeze as soon as the laser irradiation ends and results in the hill-shaped surface observed.

5. Conclusions

In view of the preceding results one can conclude that the local nonuniformities in the laser intensity distribution (as induced by means of multifaceted mirrors to reshape coherent laser beams) can translate into significant temperature differences on the irradiated surface sample. In the case of materials of a low thermal conductivity, such as glass, temperature calculations have shown the development of steep thermal gradients both on the surface and in depth, with differentiated cooling rates. Under these conditions of nonuniform thermal treatment the occurrence of effects such as nonuniform polishing have been predicted and experimentally demonstrated. Furthermore, in the case of good thermal conductors, such as metals, it has been shown that, although the induced surface thermal gradients are lower than in glass, they must be taken into consideration for the design of laser surface treatments whenever some degree of nonuniformity is to be expected in the corresponding irradiation intensity distribution.

References

1. P. W. Rodhes and D. L. Shealy, "Refractive optical systems for irradiance redistribution of collimated radiation: their design and analysis," Appl. Opt. **19,** 3545–3553 (1980).
2. W. B. Weldkamp, "Technique for generating focal-plane flattop laser beam profiles," Rev. Sci. Instrum. **53,** 294–297 (1982).
3. J. Cordingley, "Application of a binary diffractive optic for beam shaping in semiconductor processing by lasers," Appl. Opt. **32,** 2538–2542 (1993).
4. M. Duparré, M. A. Golub, B. Lüdge, V. S. Pavelyev, V. A. Soifer, G. V. Uspleniev, and S. G. Volotovskii, "Investigation of computer-generated diffractive beam shapers for flattening of single-modal CO_2 laser beams," Appl. Opt. **34,** 2489–2497 (1995).
5. S. K. Dew and R. R. Parsons, "Absorbing filter to flatten Gaussian beams," Appl. Opt. **31,** 3416–3419 (1992).
6. S. P. Chang, J. Kuo, Y. Lee, C. Lu, and K. Ling, "Transformation of Gaussian to coherent uniform beams by inverse-Gaussian transmittive filters," Appl. Opt. **37,** 747–752 (1998).
7. J. Armengol, F. Vega, N. Lupón, and F. Laguarta, "Two-faceted mirror for active integration of coherent high-power laser beams," Appl. Opt. **36,** 658–661 (1997).
8. T. Henning, M. Scholl, L. Unnebrink, U. Habich, R. Lebert, and G. Herziger, "Beam shaping for laser materials processing with non-rotationally symmetric optical elements," in *XI International Symposium on Gas Flow and Chemical Lasers and High-Power Laser Conference*, D. R. Hall and H. J. Baker, eds., Proc. SPIE **3092,** 126–129 (1997).
9. D. M. Dagenais, J. A. Woodroffe, and I. Itzkan, "Optical beam shaping of a high power laser for uniform target illumination," Appl. Opt. **24,** 671–675 (1985).
10. F. M. Dickey and B. D. O'Neil, "Multifaceted laser beam integrators," in *Current Developments in Optical Engineering II*, R. E. Fischer and W. J. Smith, eds., Proc. SPIE **818,** 94–104 (1987).
11. R. E. Grojean, D. Feldman, and J. F. Roach, "Production of flat top beam profiles for high energy lasers," Rev. Sci. Instrum. **51,** 375–376 (1980).
12. M. R. Latta and K. Jain, "Beam intensity uniformization by mirror folding," Opt. Commun. **49,** 435–439 (1984).
13. F. Laguarta, N. Lupón, and J. Armengol, "Optical glass polishing by controlled laser surface-heat treatment," Appl. Opt. **33,** 6508–6513 (1994).
14. A. Kar, J. E. Scott, and W. P. Lattann, "Effects of the mode estructure on three-dimensional laser heating due to single or multiple rectangular beams," J. Appl. Phys. **80,** 667–674 (1996) and references therein.
15. M. Von Allmen and A. Blatter, *Laser-Beam Interactions with Materials: Physical Principles and Applications* (Springer-Verlag, Berlin, 1995), Chap. 3.
16. P. Strömbek and A. Kar, "Self-focusing and beam attenaution in laser material processing," J. Phys. D **31,** 1438–1448 (1998).
17. A. García-Beltrán, "Desarrollo y validación de un modelo computacional para la predicción y caracterización de procesos de tratamiento térmico superficial de materiales con laser," Ph.D. dissertation (Universidad Politécnica de Madrid, Madrid, Spain, 1996).
18. Y. M. Xiao and M. Bass, "Thermal stress limitations to laser fire polishing of glasses," Appl. Opt. **22,** 2933–2936 (1983).
19. F. Vega, N. Lupón, J. Armengol, and F. Laguarta, "Laser application for optical glass polishing," Opt. Eng. **37,** 272–279 (1998).
20. D. A. MacGraw, "The transfer of heat in glass during forming," J. Am. Ceram. Soc. **44,** 353–363 (1961).
21. E. D. Palik, ed., *Handbook of Optical Constants of Solids* (Academic, New York, 1985).
22. E. M. Breinan and B. H. Kear, "Rapid solidification laser processing at high power density," in *Laser Materials Processing*, M. Bass, ed., Vol. 3 of Materials Processing Theory and Practices (North-Holland, Amsterdam, 1983), pp. 235–295.
23. M. Bass, ed., *Handbook of Optics II* (McGraw-Hill, New York, 1995).
24. V. P. Veiko and Y. Yakovlev, "Physical fundamentals of laser forming of micro-optical components," Opt. Eng. **33,** 3567–3571 (1994).
25. M. Wakai, Y. Komagachi, and G. Kanai, "Microlenses and microlens arrays formed on a glass plate by use of a CO_2 laser," Appl. Opt. **37,** 627–631 (1998).
26. G. Da Costa, "Competition between capillary and gravity forces in a viscous liquid film heated by a Gaussian laser beam," J. Phys. (Paris) **43,** 1503–1508 (1982).
27. J. Calatroni and G. Da Costa, "Interferometric determination of the surface profile of a liquid heated by a laser beam," Opt. Commun. **42,** 5–9 (1982).